Photopolymerization of powder suspensions for shaping ceramics

John W. Halloran [a,*], Vladislava Tomeckova [a], Susan Gentry [a], Suman Das [b], Paul Cilino [b],
Dajun Yuan [b], Rui Guo [b], Andirudh Rudraraju [b], Peng Shao [b], Tao Wu [b], Taiwo R. Alabi [b],
Wil Baker [c], Daira Legdzina [c], Dennis Wolski [c], Walter R. Zimbeck [d], David Long [d]

[a] *University of Michigan, Ann Arbor, MI 48109-2136 USA*
[b] *Georgia Institute of Technology, Atlanta, GA USA*
[c] *Honeywell Engines and Systems, Phoenix, AZ, USA*
[d] *Technology Assessment and Transfer, Annapolis, MD, USA*

Available online 30 December 2010

Abstract

The photopolymerization of suspensions of ceramic powders in monomer solutions is the fundamental step for forming techniques where a liquid suspension is solidified with UV light. The photopolymerization behavior is determined by the properties of the monomer and photoinitiator and by the transport of photons in the suspension. Photon transport in suspensions involves scattering from the particle and absorption by photoinitiators and inert dyes. The photopolymerization behavior is related to the formulation of the suspensions. Proper formulations are discussed for several applications. Techniques for characterization include cure depth measurements, photocalorimetry, and photorheology.
© 2010 Elsevier Ltd. All rights reserved.

Keywords: Photopolymerization; Shaping; Suspensions; Rapid prototyping

1. Introduction

Photopolymerizable ceramics find application in photoimageable LTCC systems,[1] patterned substrates,[2,3] dental resins,[4] the shaping of ceramics by layered manufacturing techniques[5,6] for macroscopic objects[7,8] and microfabrication.[9,10] Photopolymerizable suspensions consist of ceramic particles dispersed in a polymerizable medium, which can be aqueous or non-aqueous[11–13] with photoinitiators added to cause polymerization of the medium upon illumination. It is essentially photogelcasting, so the principles are the same as ordinary gelcasting: powders are dispersed in a high solid loading to prepare a fluid suspension that can be solidified by the gelation of the medium, combined with the well-known techniques of photopolymerization.[14]

2. Shaping with photopolymerizable suspensions

Single layers can be patterned by exposing the liquid photosuspension through a mask or with a maskless device as is done with commercial photoimageable thick films. An example of a patterned single layer is shown in Fig. 1, which is a 100-μm thick layer of silica patterned with a maskless exposure unit used in the printing industry. The solid areas were exposed, converting the fluid suspension to a solid green body. After patterning the still-fluid uncured photosuspension was rinsed away to define a pattern of holes.

Three-dimensional objects are made from many thin layers, with each layer having the pattern defined by a CAD design, with the exposure of each layer accomplished with a scanning laser[15] for stereolithography or maskless pattern.[16] Fig. 2 is a section of a silica investment casting mold fabricated from the novel method of Large Area Maskless Photopolymerization (LAMP),[17] where each layer is rapidly patterned by UV exposure in the pattern of a bitmap defined by a spatial light modulator. The bitmap for each layer is obtained by slicing the native CAD design. After exposing a layer, a thin (100 μm) fresh layer of photosuspension is deposited, and the bitmap for the next layer is patterned. The process is repeated for hundreds or thousands of layers to complete the "build", which is the shaped object of ceramic-filled photopolymer, immersed in the uncured liquid photosuspension. After completion of the "build", the photopolymerized object is separated from the uncured liquid to yield a ceramic green body, consisting of ∼60 vol% ceramic powder in a photopolymer binder. The ∼40 vol% polymer is

---
* Corresponding author at: Department of Materials Science and Engineering, University of Michigan, 2300 Hayward Street, Ann Arbor, MI 48109-2136, USA. Tel.: +1 734 763 1051; fax: +1 734 763 4788.
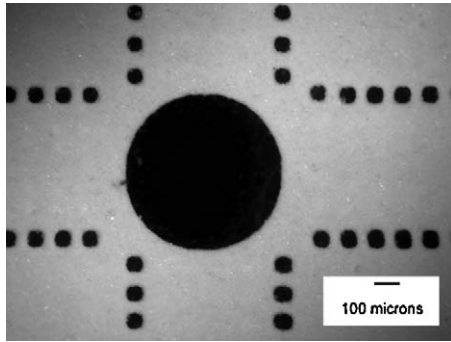   *E-mail address:* peterjon@umich.edu (J.W. Halloran).

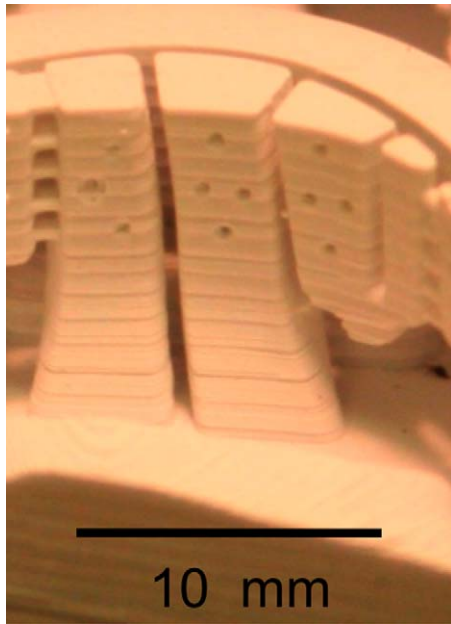Fig. 1. Single ceramic layer patterned with maskless exposure unit.

Fig. 2. Sub-millimeter features on a 40-mm tall silica ceramic component built by Large Area Maskless Photopolymerization.

Fig. 3. Silica ceramic component built by stereolithography.

removed by pyrolysis in a binder burnout step, and the ceramic is sintered using conventional methods. Similar builds can be conducted using a commercial stereolithography apparatus, where the patterning of each layer is accomplished by laser scanning. The pattern for the layer is defined as a sequence of border vectors defining the perimeter of the cured region and fill vectors, curing the inside of the perimeters. In this case the design is converted from its native CAD to an .STL file, which is subsequently sliced and converted to files that command the laser vector scans. Fig. 3 is a silica investment-casting core made by stereolithography. The stereolithography method is roughly similar to LAMP, although is expected to be significantly faster and capable of finer detail. This paper concerns these shaping methods, with emphasis on formulating and characterizing photopolymerizable suspensions.

3. Formulating photopolymerizable suspensions

As this process is photo-gelcasting, the suspensions have similar requirements. The suspension is solidified with relatively little shrinkage, so the green density of the shaped green body is determined by the volume fraction of ceramic powder Φ in the suspension. Thus suspensions must have a ceramic loading Φ ~60 vol%, and maintaining sufficiently low viscosity for convenient flow requires the use of an effective colloidal dispersant. As with all ceramic colloids, the choice of dispersant depends on the properties of the dispersed ceramic and the liquid medium. Aqueous photosuspensions often use acrylamide-based monomers similar to ordinary gelcasting, and the dispersants are similar, with similar colloidal behavior. Non-aqueous photosuspensions are often based on the less viscous acrylate monomer, such as difunctional hexane diol-diacrylate. It is in fact quite easy to disperse most oxides in acrylate monomers using commercial dispersants to achieve suspensions that appear to be quite well dispersed. These suspensions can be nearly Newtonian, with the relation between reduced viscosity and Φ can be fit[18] to the Krieger–Dougherty Equation, suggesting that the viscosity involves simple hydrodynamic flow rather than colloidal flocculation.

The novel aspect is the photopolymerization itself, which involves the use of photo-active components. These photo-active components include the following: (1) a photoinitiator, which is a dye that decomposes to form free radicals upon absorption of a UV photon, thereby initiating polymerization reactions; (2) inert dyes, which absorb photons without forming free radicals; and (3) inhibitors, which react with free radicals to inhibit polymerization. The transport of photons in a turbid suspension is strongly affected by light scattering, which can be moderated by the refractive index of the suspension. The combination of scattering and photoactive components determines the photopolymerization properties of the suspension, and the distance beneath the surface to which the polymerization reaction can occur (depth of cure) for a given exposure energy dose. The relation between the depth
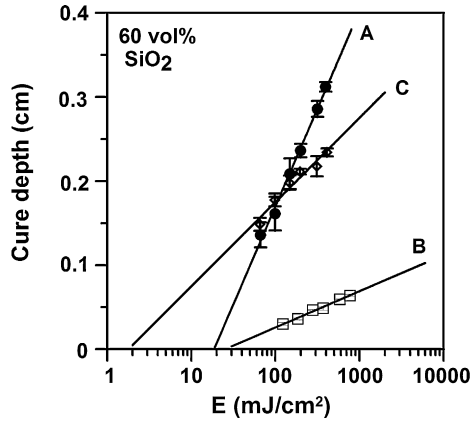
Fig. 4. Cure depth vs. energy dose for three 60 vol% silica suspensions in acrylate monomers, illustrating the effect of the concentration of the photoactive components. Data are measured values, the lines are from Eq. (2). Photosuspension A has 0.5 wt% Irgacure 184 ketone photoinitiator and no inert dye; photosuspension B has 3 wt% ketone photoinitiator and 0.15 wt% Tinuvin 171 inert dye; photosuspension C has 4 wt% Irgacure 184 ketone photoinitiator and no inert dye.

of cure, C_d, and the energy dose, E, is described by the Jacobs Equation[15]:

$$C_d = D_p \ln \left(\frac{E}{E_c} \right) \quad (1)$$

where each formulation has a particular value for the critical energy dose E_c, in joules per unit area, required for photopolymerization, and a "depth of penetration" or sensitivity parameter D_p.

3.1. Relation of cure depth to energy dose

The relation between cure depth and energy dose is commonly displayed as a semi-log plot of cure depth vs. log(E), as in Fig. 4, where D_p is the slope and E_c is the intercept on the energy dose axis. Recently predictive models were proposed[19] to describe D_p and E_c in terms of the composition and properties of the photoactive components, the ceramic particle loading, and the scattering power of the particles. For UV-transparent ceramics these expressions can be combined to relate the cure depth to the energy dose by:

$$C_d(E) = \frac{1}{1/l_{Sc} + (1 - \Phi)(c_P \varepsilon_P + c_D \varepsilon_D)}$$
$$\left(\ln E - \ln \left[(1 - \Phi) \frac{h\nu}{\Omega} (\gamma_Q Q + \gamma_D c_D) \frac{1}{\varepsilon_P c_P} \right] \right) \quad (2)$$

Here the volume fraction of ceramic is Φ, and the light scattering is quantified by a scattering length[20,21,22] l_{Sc}. Absorption by the photoinitiator, which creates free radicals for photopolymerization, is quantified by $c_P \varepsilon_P$ which is the product of the concentration (c_P) and extinction coefficient (ε_P) for the photoinitiator. Absorption by inert dyes, which absorb photons without creating free radicals, is quantified by the product $c_D \varepsilon_D$. The role of polymerization inhibitors is quantified by the concentration of inhibitors (Q) and the number of radicals consumed

per inhibitor (Q), where Ω is the quantum yield for photo generation. Usually the monomer only contains a small amount of inhibitors, sufficient to prevent dark reaction, so typically $\gamma_Q Q << \gamma_D c_D$. Each of the terms in Eq. (2) can be independently evaluated by analysis of cure depth measurements, or by direct spectrophotometry, as presented in more detail elsewhere.[23,24]

The ceramic has two roles: it attenuates the UV light by scattering through the l_{Sc} term and it dilutes the photoactive medium through the $(1 - \Phi)$ term. The photoinitiator attenuates the UV by absorption, while generating free radicals that cause the polymerization reaction. The inert dyes attenuate the UV by absorption without creating free radicals, and the inhibitors remove some of the free radicals before they can cause reaction.

3.2. Influence of the optical properties of the photoactive components

The importance of the photoactive components is illustrated in Fig. 4, which shows the cure depth vs. energy dose for three 60 vol% silica suspensions in the diacrylate monomers, cured with a 355 nm UV laser. These suspensions have different concentrations of photoactive components. The data points are the measured values of cure depths for the three different formulations. The lines through the data are calculated from the model with Eq. (2). The parameters used in the Eq. (2) lines are[23]: $\varepsilon_P = 189$ L/(mole-cm) for the molar extinction coefficient of the photoinitiator, $\varepsilon_D = 25,600$ L/(mole-cm) for the molar extinction coefficient of the inert dye, with $l_{Sc} = 0.116$ cm for the scattering length. The values for the inhibitor parameters are[24]: $(h\nu/\Omega)(\gamma_Q Q + \gamma_D c_D)/\varepsilon_P = 1.25$ (mJ-mol)/(L-cm²) and $(h\nu/\Omega)(\gamma_D/\varepsilon_P) = 1465$ mJ/cm².

These three formulations behave quite differently. Line A in Fig. 4 is for a suspension with 0.5 wt% of Irgacure 184, a ketone photoinitiator. This suspension has a sensitivity D_p of 1010 μm and a critical energy dose E_c of 18.0 mJ/cm². For this case achieving a cure depth C_d of 0.05 cm requires an energy dose of only 30 mJ/cm². The cure depth is much lower for a suspension shown by Line B in Fig. 4, which is formulated with higher photoinitiator concentration (3%) and includes a 0.15% of an intensely absorbing inert dye (Tinuvin 171). To achieve a 0.05 cm cure depth for suspension B, the dose must be 300 mJ/cm², since the Jacobs parameters are quite different, with D_p of 188 μm and an E_c of 25.2 mJ/cm².

The cure depth C_d must be at least equal to the thickness that is to be cured. The appropriate values for the D_p and E_c depend upon the requirements. A large D_p and small E_c are appropriate for curing thick single layers with low energy dose. For such a case, dyes are to be avoided and the concentration of photoinitiator is chosen for the desired balance of sensitivity and critical energy. This is illustrated by the suspension shown in Line C in Fig. 4, which is similar to the Line A suspension, but with a higher concentration of the photoinitiator, 4%. This causes the slope to be smaller (D_p of 435 μm) and the intercept to be smaller ($E_c \sim 2$ mJ/cm²), compared to the formulation with less photoinitiator in Line A. For cure depths thinner than 0.15 cm, suspension C with 4% photoinitiator requires a

smaller energy dose than suspension A with 0.5% photoinitiator. If thicker cure depths are desired, suspension A with 0.5% photoinitiator requires a smaller energy dose.

However, energy dose is not the only concern for formulating a photopolymerizable suspension. When building with multiple layers for rapid prototyping, the cure depth C_d must be accurately matched to the layer thickness λ. Typically, C_d should be equal to the layer thickness plus a certain amount of over cure (OC) to assist in bonding of the layers: $C_d = \lambda + OC$. If the cure depth is too large, $C_d > \lambda + OC$, there will be undesirable "print-through" which will reduce the accuracy of the build. Typically the over cure should be about 10–35% of the layer thickness to avoid print-through while also avoiding delamination. Small cure depth could be achieved with small energy dose if the D_p is large, but it could also be achieved with a larger energy dose if the D_p is smaller. For laser stereolithography, where the object is a series of layers about 100 μm thick, a small D_p is preferred, since the laser beam power is not perfectly stable. The power of a typical UV laser fluctuates[25] about 3–5% during a scan. This power fluctuation causes an energy dose fluctuation δE at particular locations, resulting in a local cure depth fluctuation $\delta C_d \sim (D_p/E)\delta E$. For a photosuspension with a high sensitivity, like Line A of Fig. 4, a 5% variation in laser power can result in a variation of cure depth of about 50 μm, while a lower sensitivity photosuspension like Line B would only have about a 10 μm variation in cure depth. So a photosuspension with a smaller D_p is preferred for builds with thin layers, such as those used to achieve high resolution features.

Smaller D_p is also improves lateral (x–y) resolution. Depending on the exposure technique, the edges of fine features are defined by hard masks, by maskless systems, or by laser scanning. In all these cases, lateral spreading of the UV beam in the photosuspension degrades the sharpness of the edge. Side scattering is a prominent cause of lateral spreading for photosuspensions, since the ceramic particles often have a higher refractive index than the suspension medium, as expressed by the refractive index contrast Δn. The scattering contribution to lateral spreading depends upon refractive index contrast and the D_p. Better spatial resolution is expected when the attenuation from scattering is smaller then attenuation from absorption. Formulations with a small, absorption-dominated D_p, such as Line B in Fig. 4, are favored for higher resolution.

3.3. Influence of the optical properties of ceramic

For a given set of photoactive dyes and photoinitiators, the cure depth at any energy dose depends on the refractive index contrast Δn. Griffith[26] measured the cure depth of a series of 50 vol% silica suspensions in an aqueous photosuspensions, cured with a 351 nm Ar-ion UV laser. The refractive index of the solutions depended upon the concentration of monomer (acrylamide and methylene bisacrylamide) in the water, and the presence of ethylene glycol. Fig. 5 shows that the cure depth at a constant dose of 1500 mJ/cm² varies linearly with the $1/(\Delta n)^2$. For UV-transparent ceramics, those with low refractive index, such as fused silica ($n = 1.45$), quartz ($n = 1.56$) or alumina ($n = 1.70$) have a relatively small refractive index contrast
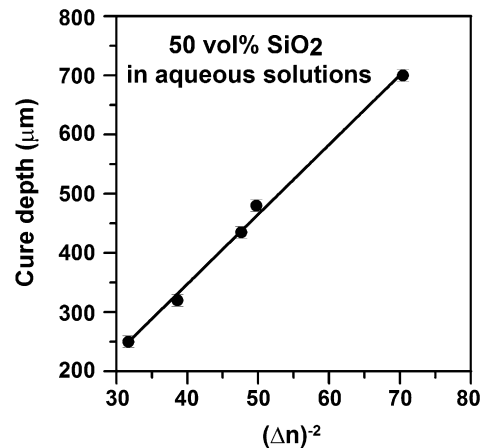

Fig. 5. Cure depth at constant UV dose of 1500 mJ/cm² for 50 vol% silica suspensions in a solution of water, ethylene gycol, acrylamide and methylene bisacrylamide, showing the effect of refractive index contrast between the powder and the liquid.

with diacrylates like hexane diol diacrylate ($n = 1.457$) or aqueous acrylamide solutions (1.382 for 70% water). High refractive index UV-transparent ceramics like zircon ($n = 2.00$) or zirconia ($n = 2.20$) require a large energy dose for a significant cure depth.

Many ceramics are UV-transparent, but there are prominent examples such as SiC, TiO₂ and the titanates, where the UV absorption edge occurs at energies smaller than the UV photons. For ceramics that absorb UV, the extinction coefficient of the ceramic itself at the UV wavelengths has to be considered, so the denominator of Eq. (2) has to be changed from:

$$\frac{1}{l_{Sc}} + (1 - \Phi)(c_P \varepsilon_P + c_D \varepsilon_D)$$

which is the form appropriate for transparent ceramics to include the absorption of a ceramic as:

$$\frac{1}{l_{Sc}} + \Phi \rho_{cer} \varepsilon_{cer} + (1 - \Phi)(c_P \varepsilon_P + c_D \varepsilon_D)$$

Here the term ε_{cer} is the extinction coefficient of the ceramic at the UV wavelengths of the source. The concentration of the ceramic in the suspension (in g/cm³), is $\Phi \rho_{cer}$, the product of the volume fraction of the ceramic and its density. Monomers such as hexane dioldiacrylate are quite transparent for wavelengths longer than 360 nm, but similar terms could be added if the monomers have significant absorption.

3.4. Influence of the UV source

The appropriate values for the extinction coefficients have to be evaluated for the particular UV source. Each source has its particular emission spectrum, and absorbance (the product of concentration and extinction coefficient ($c\varepsilon$)) of the photoactive components is a strong function of wavelength. Fig. 6 is an example of the absorption spectra of the photoinitiator Irgacure 184 and inert dye Tinuvin 171. These photoactive agents are designed to absorb over a particular range of wavelengths and typically have quite complicated absorption spectra.
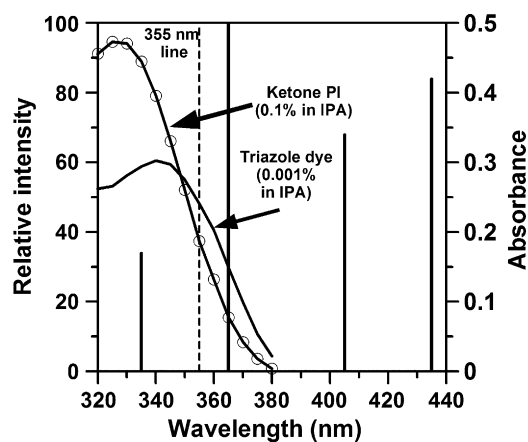
Fig. 6. Comparison of the absorption spectra of the ketone photoinitiator Irgacure 184 and the UV absorber dye Tinuvin 171 with the emission spectrum of the mercury vapor lamp in a PhotoDSC apparatus. Note that the dye and photoinitiator are sensitive to the 335 nm and 365 nm lines, but insensitive to the 405 nm and 431 nm lines. The 355 nm laser emission is shown as a dashed line.

The emission spectra of UV sources vary widely, from single wavelengths in lasers to multiple emission lines in lamp sources. For single emission line sources, the extinction coefficient that appears in Eq. (2) is simply the value of ε at the laser wavelength. For multi-line spectra, such as the mercury vapor lamp spectrum shown in Fig. 6, the appropriate extinction coefficient should be found by convoluting the absorption spectrum with the emission spectrum. For the example of Fig. 6, this involves the absorbance at the 335 nm line multiplied by the relative intensity of the 335 line combined with the absorbance at the 365 nm line multiplied by the relative intensity of the 365 line. The emission lines at 405 and 435 nm play no role, since they are not absorbed. With the convoluted extinction coefficient, it is possible to compare curing behavior for different UV sources.

4. Characterizing photopolymerizable suspensions

4.1. Cure depth measurements

The most direct characterization of the photopolymerization behavior is through measurement of the cured depth as a function of energy dose, to obtain data like Fig. 4. This can be done by exposing a thick layer of liquid photosuspension to known doses of UV energy, removing the solidified layer, and measuring the C_d with a micrometer. Alternately, one could program a stereolithography or LAMP apparatus to deliver a series of doses in a test pattern. Reliable measurements require careful technique for rinsing the uncured photosuspension and measuring the thickness of the cured layer. This involves measurements on thin layers of rather soft green ceramics, so reproducibility of the C_d is typically about ±5%. Layered manufacturing applications typically use layers on the order of 100 μm thick, but these are too thin and fragile to measure the C_d directly. Instead larger energy doses are used to produce C_d values in the range of 0.05–0.5 cm, where the thickness can be measured more easily. Thus the working parameter for ∼100 μm layers,

$E(C_d = 100 \, \mu\text{m})$ is obtained by extrapolation of a regression line on a semilog plot. A modest amount of scatter in the cure depth values $C_d \pm \delta C_d$ can lead to considerable uncertainty in the slope of the regression line slope D_p and intercept $\ln(E_c)$, resulting in uncertainty in the values for the photosuspension parameters sensitivity $D_p \pm \delta D_p$ and critical energy $\ln E_c \pm \delta \ln E_c$. The error range in the $\ln E_c$ makes the linear error limits on the critical energy quite uneven, as $E_c + \delta E_c$(upper limit) $- \delta E_c$(lower limit).

4.2. Calorimetry and spectroscopy

Polymerization reactions are exothermic and the reaction enthalpy is usually well known, so reaction kinetics can be easily characterized by differential scanning calorimetery[27] (DSC). For photopolymerization, the DSC is modified for the photoDSC technique[28] to illuminate a thin sample, ideally thinner than D_p so the cure reaction is uniform through the thickness, and measuring the enthalpy as a function of time during illumination. The behavior of unfilled monomers like diacrylates is well known,[29] and ceramic-filled monomers behave similarly.[30,32] The thermal heat output is measured as a function of time during illumination with a known UV power. Thermal heat is converted to polymerization rate, R_p, using the known enthalpy of polymerization, which is integrated to give the extent of reaction, α, as a percent of conversion of the C=C bonds. Illumination time is converted to energy dose to display R_p vs. dose and α vs. dose. Fig. 7 shows photoDSC results for a 60 vol% silica suspension with no UV absorber dye as a plot of polymerization rate and extent of reaction vs. dose for two concentrations of photoinitiator, showing the typical behavior for autocatalytic free radical polymerizations. Notice that the reaction occurs at smaller energy doses at higher photoinitiator concentration, as the UV photons create more free radicals. Also note that only about 80% of the C=C bonds are reacted during photopolymerization as radicals are "frozen" in the gel.[31] PhotoDSC can be complemented by infrared spectroscopy. Real time FTIR is a convenient characterization method to follow the polymerization by the disappearance of the C=C IR bands,[33] which can be also applied to ceramics.[34]

4.3. Rheometry

Photopolymerization can also be characterized by chemorheology, using photorheometry. For this, one of the plates of a parallel plate rheometer is transparent and illuminated with a well-characterized UV source. A thin sample (again thinner than D_p) is exposed to a know UV intensity, and the dynamic viscosity is measured as a function of time during illumination. Polymerization kinetics[35] can be inferred from the photorheological behavior. Fig. 8 shows photorheometry data for a 60 vol% silica suspension in a diacrylate, as a plot of torque for oscillatory excitation in the linear range as a function of time for three levels of intensity. Further details are reported elsewhere.[36] Typically there is an induction period, followed by rapid increase in torque as the suspension gels. In this case for the diacrylate monomers, the differences in the rise of torque vs. time scales simply with UV intensity, as would be expected if the UV dose required for
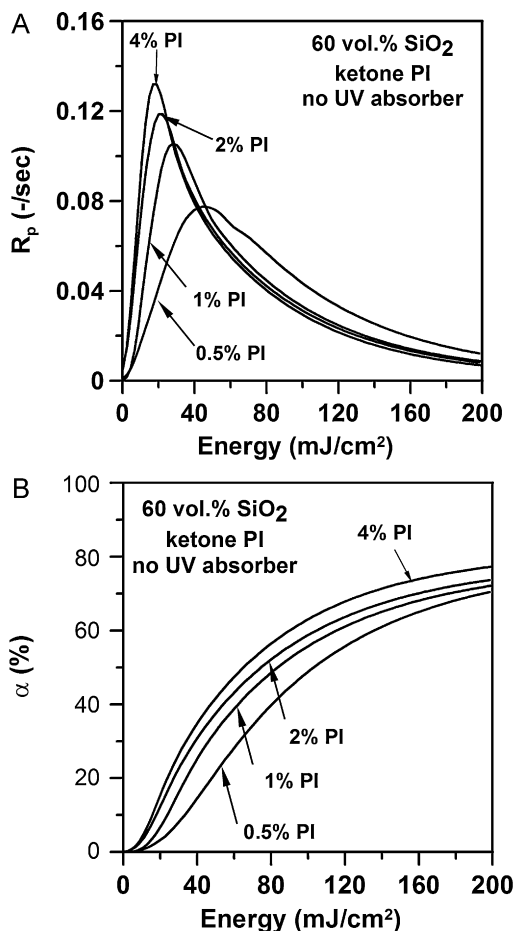
Fig. 7. Characterization of photopolymerization by photo DSC showing faster polymerization of a 60 vol% suspension of silica in acrylate monomers with 4 wt% Irgacure 184 ketone photoinitiator vs. 0.5 wt% as polymerization rate (A, top) and extent of reaction (B, bottom).

curing is independent of intensity. In other cases, such as glycol dimethacrylate monomers, which have slower polymerization kinetics, the cure dose varies significantly with intensity, with smaller cure doses required for lower intensities.[36]
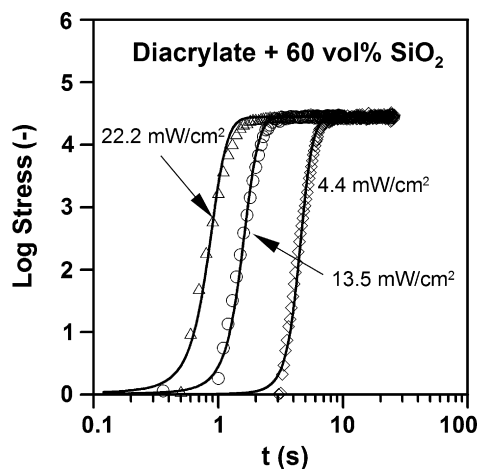

Fig. 8. Photorheology of diacrylate suspension (60 vol% SiO$_2$) with 2% photoinitiator showing oscillatory torque as a function of illumination time at 3 different light intensities 4.4, 13.5 and 22.2 mW/cm^2.

5. Conclusions

The formulation of photopolymerizable suspensions changes the behavior by a combination of absorption, scattering, and inhibition. The ceramic particles dilute the photoactive components in the monomer solution that absorb UV, but also limit UV penetration by scattering to a degree dependent on the refractive index contrast. The photoinitiators attenuate the UV by absorption, while producing free radicals for polymerization. Inert dyes cause further absorption, but do not produce free radicals. Inhibitors remove free radicals. The relationship between energy dose and cure depth can be adjusted in predictable ways through the formulation. The photopolymerization behavior can be characterized by direct cure depth measurements, by calorimetry, and by photorheology.

Acknowledgements

References

1. Taylor BE, Bidwell L, Lawrence A. New photoimageable LTCC technology for making a wide range of ceramic architectures and circuits international conference on high density interconnect and systems packaging. In: *SPIE Proceedings, vol. 4428*. 2001. p. 89–92.
2. Lee HD, Pober RL, Calvert PD, Bowen HK. Photopolymerizable binders for ceramics. *J Mater Sci Lett* 1986;**5**:81–181.
3. Zimbeck WR, Jang JH, Schultze W, Rice RW. Automated fabrication of ceramic electronic packages by stereo-photolithography. In: Danforth SC, Dimos DB, Prinz F, editors. *Solid Freeform and Additive Fabrication-2000, Materials Research Society Proceedings, vol. 625*. 2000. p. 173–8.
4. Lovell LG, Lu H, Elliot JE, Stansbury JW, Bowman CN. Effect of curing rate on the mechanical properties of dental resins. *Dent Res* 2001;**17**(6):504–11.
5. Halloran JW, Bae C-J, Torres-Garibay C, Tomeckova V, Das S, Baker W. Manufacture of complex ceramics by photopolymerization. In: Bellosi A, Nicola Babini G, editors. *Global Roadmap for Ceramics-ICC2 Proceedings, Proceedings of the 2nd International Congress on Ceramics*. 2008. p. 369–78, published by Agenzia Polo Ceramico S.C. A.r.l., Faenza, Italy, ISBN 978-88-8080-084-2.
6. Doreau F, Chaput C, Chartier T. Stereolithography for manufacturing ceramic parts. *Adv Eng Mater* 2000;**2**(8):493–4.
7. Bae C-J, Halloran JW. Integrally cored ceramic mold fabricated by ceramic stereolithography. *Int J Appl Ceram Technol* 2010 (ACT 1131. R1).
8. Esposito Corcione C, Greco A, Montagna F, Lucciulli A, Maffezzoli A. Silica moulds built by stereolithography. *J Mater Sci* 2005;**40**:4899–904.
9. Sun C, Zhang X, Experimental. Numerical investigations on microstereolithography of ceramics. *J Appl Phys* 2002;**92**(8):4796–7.
10. Bertsch A, Jiguet S, Renauld P. Microfabrication of ceramic components by microstereolithography. *J Micromech Microeng* 2004;**14**:197–203.
11. De Hazan Y, Heinecke J, Weber A, Graule T. High solids loading ceramic colloidal dispersions in UV curable media with via comb-polyelectrolyte dispersants. *J Colloid Interface Sci* 2009;**337**(September (1)):66–74.
12. Zhou W, Li D, Wang H. A novel aqueous ceramic suspension for ceramic stereolithography. *Rapid Prototyping J* 2010;**16**(1):9–35.
13. Griffith ML, Halloran JW. Freeform fabrication of ceramics by stereolithography. *J Am Ceram Soc* 1996;**79**(10):2601–8.

14. Bowman CN, Kloxin CJ. Toward an enhanced understanding and implementation of photopolymerization reactions. *AIChE J* 2008;**54**(11):2775–95.

15. Jacobs PF. Rapid prototyping & manufacturing-fundamentals of stereolithography. *Soc Manuf Eng* 1992.

16. Ventura SC, et al. A new SFF process for functional ceramic components. In: Bourell D, et al., editors. *Solid Freeform Fabrication Symposium Proceedings*. 1996. p. 327.

17. Yuan D, Kambly K, Shao P, Rudrarju A, Cilio P, Tomeckoa V, et al. Experimental investigations on photocurable ceramic materials systems for large area maskless photopolymerization (LAMP). In: Bourell D, et al., editors. *Solid Freeform Fabrication Symposium Proceedings SFF-'09*. 2009.

18. Tomeckova V, Halloran JW. Flow behavior of polymerizable ceramic suspensions as a function of ceramic volume fraction and temperature (this conference). *J Eur Ceram Soc* 2010.

19. Tomeckova V, Halloran JW. Predictive models for the photopolymerization of ceramic suspensions. *J Eur Ceram Soc* 2010;**30**:2833–40.

20. Lee JH, Prud'homme R, Aksay IA. Cure depth in photopolymerization: experiments and theory. *J Mater Res* 2001;**16**(12):3536–44.

21. Garg R, Prud'homme R, Aksay I, Liu A, Alfano R. Adsorption length for photo propagation in highly dense colloidal dispersions. *J Mater Sci* 1998;**13**(12):3463–7.

22. Wu KC, Seefeldt KF, Solomon MJ, Halloran JW. Prediction of ceramic stereolithography resin sensitivity from theory and measurement of diffusive photon transport. *J Appl Phys* 2005;**98**(July). p. 024902-1–10.

23. Tomeckova V, Halloran JW. Cure depth for photopolymerization of ceramic suspensions. *J Eur Ceram Soc* 2010;**30**:3023–33.

24. Tomeckova V, Halloran JW. Critical energy for photopolymerization of ceramic suspensions. *J Eur Ceram Soc JECS-S-10-00296* 2010;**30**:3273–82.

25. Gentry SP, Baker W, Legzdina D, Wolski D, Zimbeck W, Halloran JW. Resolving fine features using ceramic stereolithography. In: *presented at MS&T 2009*. 2009.

26. Griffith ML. Stereolithography of ceramics. Ph.D. thesis. University of Michigan; 1995.

27. Chu TM, Halloran JW. Curing of highly loaded ceramics in acrylates. *J Am Ceram Soc* 2000;**83**(10):2075–80.

28. Hoyle CE. In: Pappas SP, editor. *Radiation curing: science and technology*. New York: Plenum Press; 1992. p. 61.

29. Hoyle CE, Cramford M, Trapp M, No YG, Kim K-J. Photopolymerization of 1,6-hexanediol diacrylate with deoxybenzoin as a photoinitiator. *Polymer* 1988;**29**:2033–40.

30. Brady GA, Halloran JW. Differential photo-calorimetry of photopolymerizable ceramic suspensions. *J Mater Sci* 1998;**33**:4551–60.

31. Kloosterboer JG. Network formation by chain crosslinking photopolymerization and its applications in electronics. *Adv Polym Sci* 1988;**84**:1–61.

32. Kambly K. Characterization of curing kinetic and polymerization shrinkage in ceramic-loaded photocurable resins for Large Area Maskless Photopolymerization (LAMP). MS Thesis. Atlanta, GA: School of Mechanical Engineering, Georgia Institute of Technology; 2009.

33. Anseth KS, Bowman CN, Peppas NA. Polymerization kinetics and volume relaxation behavior of photopolymerized multifunctional monomers producing highly crosslinked networks. *J Polym Sci Part A: Polym Chem* 1994;**32**(1):139–47.

34. Wu KC, Halloran JW. Photopolymerization monitoring of ceramic stereolithography resins by FTIR methods. *J Mater Sci* 2005;**40**:71–6.

35. Love BJ, Piguet Ruinet F, Teyssandier F. Chemorheology of photopolymerizable acrylates using a modified Boltzman sigmoidal model. *J Polym Sci Part B: Polym Phys* 2008;**46**(3):2319–25.

36. Tomeckova V, Teyssandier F, Torres-Garibay C, Love BJ, Halloran JW. Light intensity effects on the photorheology of photopolymerizable ceramic suspensions; in preparation.